Interfacial Electrochemistry in Liquids Probed with Photoemission Electron Microscopy

Slavomír Nemšák,[†] Evgheni Strelcov,*,[‡] Tomáš Duchoň,[**] Hongxuan Guo,*,[‡] Johanna Hackl, [†] Alexander Yulaev,*,[‡] Ivan Vlassiouk,[§] David N. Mueller,[†] Claus M. Schneider,[†] and Andrei Kolmakov*

[†]Peter-Grünberg-Institut 6, Forschungszentrum Jülich GmbH, 52425 Jülich, Germany

*Center for Nanoscale Science and Technology, NIST, Gaithersburg, MD 20899, USA

[‡]Maryland NanoCenter, University of Maryland, College Park, MD 20742, USA

[**]Faculty of Mathematics and Physics, Charles University, 180 00 Prague, Czech Republic

[§]Oak Ridge National Laboratory, Oak Ridge, TN 37831, USA

Supporting Information Placeholder

ABSTRACT: Studies of the electrified solid-liquid interfaces are crucial for understanding of the biological and electrochemical systems. Until recently, the use of photoemission electron microscopy (PEEM) for such purposes has been hampered by the incompatibility of the liquid samples with ultrahigh vacuum environment of the electron optics and detector. Here we demonstrate that the use of ultra-thin electron transparent graphene membranes, which can sustain large pressure differentials and act as a working electrode, makes it possible to probe electrochemical reactions *in operando* in liquid environments with PEEM.

The processes at solid-liquid interfaces are of crucial importance in environmental and bio-medical sciences, energy conversion and storage, corrosion, plasmonics and catalysis. From the electrochemical point of view, the interface between the electrode and electrolyte determines properties of an electrochemical device and its behavior, i.e. its performance and durability. Even though these interfaces have been studied for two centuries now, several new techniques have emerged in the last decades to clarify their fundamental properties[1]. Ambient pressure photoelectron spectroscopy[2] has just recently been employed to directly probe the potential and chemical profiles in an electrical double layer with sub-nanometer depth resolution.[3-5] Photoemission electron microscopy (PEEM) is a well-established and powerful technique with an irreplaceable position in the fields of surface chemistry, micromagnetism, ferroelectrics, multi-ferroics and other disciplines, where spatially resolved chemical, electrical, and magnetic information is of essence[6]. Until recently, PEEM was excluded from studies of solid-liquid interfaces due to major instrumental and experimental difficulties to implement the common differential pumping approach [7] [8]. Earlier attempts to investigate the solid-liquid interfaces in PEEM utilized thin silicon nitride films to isolate liquid inside the cell, and the PEEM measurements were built to operate in the transmission mode.[9,10] Consequently, they suffered from a limited spectroscopic window and were yielding X-ray absorption (XAS) of the bulk rather than probing the solid-liquid interface. One of the ways to overcome these problems in photoemission spectromicroscopy is to build a liquid cell capped with an electron transparent molecularly impermeable membrane.[11] First successful imaging of a liquid and solid-liquid interface in PEEM was demonstrated by the same group just recently.[12] Here, we advance this work to the next level by adding the electrical contacts to the cell, which opens yet another possibility – *in operando* electrochemistry of liquids in PEEM.

The multi-channel array (MCA) liquid sample platform[12] is a 500 μm thick glass substrate with thousands of ordered channels with a diameter of 5 μm. The front (imaging) and back sides of the MCA were coated with thin gold and platinum films (40 nm), respectively, penetrating ≈ 3 μm (Au) and ≈ 200 μm (Pt) deep into the channels. The MCA samples were filled with 0.1-0.5 mol/L solution of $CuSO_4$ balanced with 0.1 mol/L of H_2SO_4. The electrolyte concentration was preserved within 30 % of its nominal value within the channels. We note however that subsequent slow leakage of water into the chamber vacuum and X-ray induced radiolysis may alter the electrolyte composition[13]. A bilayer graphene membrane adhered to the gold coating served as a working electrode (WE), (see Fig. 1a). The Pt coating served as the counter (CE) and the pseudo-reference electrodes. The potential window (±1 V vs. Pt) was chosen to minimize electrodeposition of copper and avoid water electrolysis.

The aberration-corrected photoemission microscope was operated using an extractor voltage of -6 kV and collecting secondary electrons in a partial electron yield mode with a

bandwidth of $\approx$10 eV. *In-situ* electrochemical cycling of the liquid cell was performed by a remotely controlled potentiostat with $\approx$10 pA resolution. The top graphene electrode of the cell was connected to the sample "ground" potential of the microscope, the potentiostat applied a voltage bias to the bottom Pt counter electrode. The time resolution of the experiment is only limited by the CCD camera read-out and signal/noise ratio of the collected images; in experimental setup used it can reach 10 Hz.

We employed UE56/1-SGM soft X-ray beamline of the BESSY-II synchrotron for this study. A schematic of the experiment is shown in Figure 1a. X-ray absorption edges used for a chemical analysis were oxygen K-edge at $\approx$530 eV and copper L-edge at $\approx$930 eV. The overall energy resolution was 300 meV at oxygen K-edge and 550 meV at copper L-edge. More details on the experimental setup, energy calibration and methods used can be found in the Methods section of the supporting information file (SI).

Figure 1b shows copper L_3-edge XAS spectra averaged over the central part of one of the electrolyte-filled channels. Based on prior research[14-16], the spectra feature two peaks at 930.8 eV and 932.5 eV that can be assigned to bivalent and monovalent copper ions, or metallic copper. However, copper ions in different chemical surroundings (hydrated vs. anhydrous, surface-adsorbed vs. free ions) may have absorption spectra shifted relative to each other. To account for these possibilities, we performed comparative XAS study for solid CuO and Cu_2O,[14-16] as well as for hydrous and anhydrous $CuSO_4$[17] (see SI, Fig. S1). The XAS spectra of cuprous oxide and metallic copper have very close main edge peaks, but they can be discriminated based on the shape of the Cu^0 spectrum, which contains an extended post-edge band consisting of several secondary peaks forming an oscillatory structure of transitions into a continuum of unoccupied states. The Cu_2O spectrum has only a very weakly-defined post-edge tail (see SI). Since the peaks in Figure 1b do not have extended post edge structure we may assign them to Cu^+, or Cu^{2+}, not metallic copper. Moreover, these spectra were collected from the central part of the graphene membrane, where copper nucleation is hampered (see discussion below) and where we don't expect a pronounced electrodeposition of metallic copper. Comparison of the spectra of solid anhydrous copper (II) sulfate and its pentahydrate shows that hydration does not appreciably shift the Cu-L_3 edge absorption. All these support the assignment of the 930.8 eV peak to Cu^{2+} and the 932.5 eV one to Cu^+ ions in solution.

Variation of the WE potential leads to redistribution of peak intensities and a systematic shift of the Cu^+ peak position (Fig. 1b). An increase of the potential from 0 V to 1 V significantly reduces the bivalent peak, whereas a subsequent decrease in potential back to 0 V and, further, to -1 V, enhances it and suppresses the Cu^{2+} signal. This process is shown more quantitatively in Figure 1c, which plots areas of the individual fitted peaks normalized to the total spectral area. The presented data, thus, reflect the ratio of Cu^{2+}/Cu^+ concentrations within the probing depth of PEEM – several molecular layers deep beneath the graphene membrane, since the information depth of X-ray absorption measured via partial/total electron yield is on the order of a few nm. Originally (although after several forming voltammetric cycles), the Cu^{2+} fraction is $\approx$ 60 %. It

rapidly increases with positive applied voltage, at the expense of monovalent copper, reaching 84 % at +1 V, and then decreases to $\approx$ 50 % on potential reversal back to 0 V. In the cathodic region, the fraction of bivalent copper remains nearly unchanged.
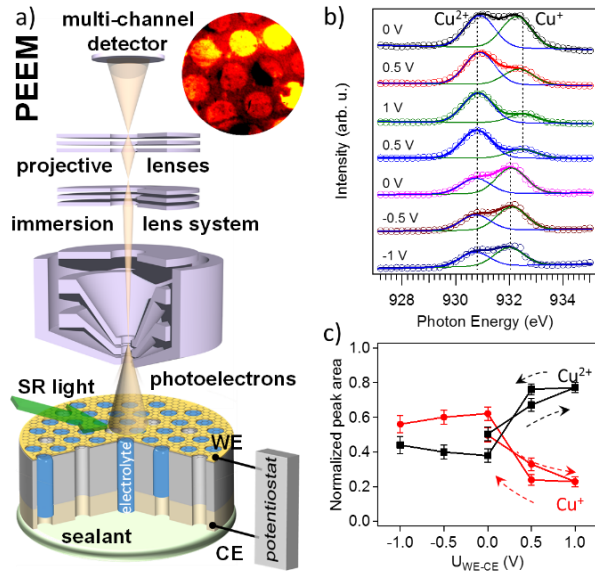

Figure 1. (a) A schematic of the PEEM electrochemical setup; Inset: PEEM image of the graphene capped MCA at the O K-edge energy. Electrolyte filled channels appear brighter compare to dry ones. (b) Averaged XAS Cu L_3-edge spectra (and their Voigt fits) collected from a graphene-capped channel filled with 0.1 mol/l $CuSO_4$ solution; spectral peaks reflect changes in concentration of the mono and bivalent copper ions just below the graphene membrane as a function of its potential; spectra are y-offset for clarity; (c) Normalized area of the fitted Cu peaks from (b), plotted against the WE potential; arrows indicate sequence of measurements. The error bars represent standard deviations and were calculated as specified in the SI.

In order to observe the electrochemically induced changes with higher potential resolution, the excitation photon energy was locked at the Cu^{2+} L_3-edge (931 eV) and PEEM imaging of a new sample region was performed as 3 voltammetric cycles were sequentially recorded. The obtained 3-dimensional dataset (partial electron yield intensity at the Cu^{2+} peak I as a function of time and x-y spatial position) cannot be directly visualized in printed form. Therefore, it was unmixed into two components, using the Bayesian Linear Unmixing algorithm (BLU).[18,19] The BLU method splits the PEEM dataset into a linear combination of user-defined number of position-independent spectral components (endmembers - S) and corresponding abundance maps (A), simultaneously filtering out noise (N): $I(x,y,t) = S(t) \cdot A(x,y) + N$. Spectral endmembers can be functions of time or energy, depending on the original dataset configuration. For detailed description of BLU, see Ref.[19]

Figure 2 shows abundance maps of the electrochemically active component (2a) and background (not active) component (2d) obtained by BLU-treating the temporal PEEM dataset recorded at the photon energy of 931 eV. The background component is due to the detector aperture (the red frame) and empty MCA channels. The electrochemically active component is localized in several electrolyte-filled cells (small red circles in the upper right of Fig. 2a). The background spectrum

2

(Fig. 2e) has a low intensity, which does not vary with time (and voltage). On the contrary, the electrochemical component temporal spectrum has an order of magnitude higher intensity and exhibits a strong correlation with the WE potential. Similar to Figure 1c, we observe a 3 % increase of the Cu^{2+} signal at the positive potential. The same temporal spectral endmembers are plotted in Figure 2c and 2f against potential and compared to the cyclic voltammograms (CV) recorded for the whole device. The onset of a rapid increase in the PEEM intensity of the electrochemical endmember coincides with the initial current rise of the anodic CV peak. The cathodic CV peak is not correlated to the endmember, whose intensity is constant in the negative potential region.

A Cu L_3-edge spectral PEEM imaging dataset of the same region recorded prior to voltage cycling was BLU-unmixed into two components shown in Figure 2g-j. Again, the background abundance map (Fig. 2i) highlights the detector aperture and empty channels, and its endmember (Fig. 2j) is featureless. The electrolyte component abundance map (Fig. 2g) shows a bright yellow pattern, where the solution-filled channels cluster, and a part of the MCA frame, where the solution is trapped at the interface between the graphene and gold coating, which increases the electron yield. The corresponding endmember energy spectrum (Fig. 2h) comprises one peak around 931 eV with a shoulder at higher photon energy side, which can be identified as weakly-resolved bi- and monovalent copper peaks similar to those present in the Figure 1b spectra, however in this case present in a large number of channels, comparing to the single channel analysis in Fig. 1b and 1c.
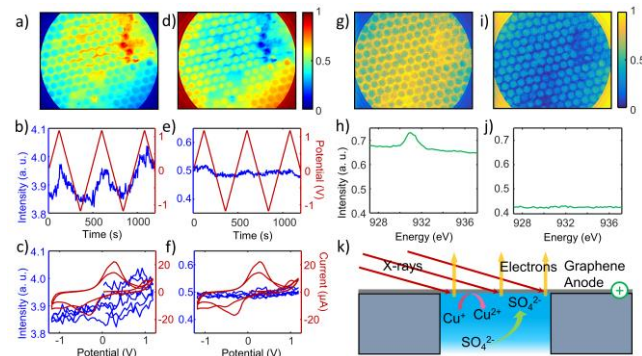

Figure 2. Copper L_3-edge data. Temporal dataset: (a) and (d) are the BLU extracted abundance maps of the electrochemically active and background components, respectively; (b) and (e) are the corresponding BLU endmember components (PEEM intensity vs. time) plotted together with the WE potential variation; (c) and (f) are the same endmembers plotted vs. voltage and 2.5 cycles of CV's recorded for the whole sample; the first cycle CV peaks are at 0.25 V and -0.53 V, for the second cycle peaks are at 0.28 V and -0.31 V; Spectral dataset: (g) and (i) are the BLU extracted abundance maps of a spectral dataset for the copper and background components, respectively; (h) and (i) are the corresponding BLU endmember spectra; (k) A schematic of the anodic processes on the WE (graphene): copper oxidation and sulfate ion adsorption.

The presented observations can be interpreted in the light of the well-studied copper electroplating process. In general, copper reduction proceeds in two Marcus steps:[20]

$$Cu^{2+} + e^- \rightarrow Cu^+ \ (slow) \tag{1}$$

$$Cu^+ + e^- \rightarrow Cu^0 \ (fast) \tag{2}$$

In non-complexing media, such as sulfuric acid, the rates of the two steps are incomparable, and the Cu^+ ion, being thermodynamically unstable,[21] becomes undetectable by standard CV methods. However, more sophisticated techniques, such as rotating disk-ring electrode, allow direct measurement of the Cu^+ concentration at a given electrode potential.[22] In addition, it is known that trace (parts per million) amounts of Cl- and sulfide-containing contaminants can stabilize monovalent copper and leave a footprint in the CV in the form of a small pre-deposition peak.[22,23] The main cathodic and anodic peaks of the recorded voltammograms of Figure 2c and 2f are separated by about 0.6 V. This fact and other measurements (see SI) allows identifying them as arising from the reversible copper deposition and electroplating processes, notwithstanding the absence of a true reference electrode in our setup (presumably, the Pt CE gets copper plated over several CV cycles, and this Cu plating serves as a pseudo-reference electrode). The peaks' broadness implies contributions from both reactions (1) and (2). Note, that electrodeposition (Eq. 2) necessarily proceeds via a nucleation step, and thus its rate depends on the electrode material. In our setup, copper nucleation is hampered on the high-quality graphene membranes, and in the potential range ±1 V mostly happens on the MCA channel's periphery, specifically on the gold-coated walls (see Fig. S1c,d in SI).[24] On the other hand, reduction reaction (1) takes place on the whole available surface area of the WE, and graphene facilitates homogeneous electrochemical reduction reactions as compared to graphite.[25] Thus, we can conclude that the concentration of Cu^+ beneath the graphene membrane can be high enough for direct spectroscopic detection due to low nucleation rate and possible influence of contaminants. In addition, it has been previously shown,[26] that during reduction of Cu^{2+} in acidic solutions containing sulfate ions, 13 to 24 monolayers of monovalent copper ions can get adsorbed on a glassy carbon electrode. Taking into account that the PEEM probing depth is on the same length-scale, the observed high Cu^+/Cu^{2+} ratio (Fig. 1c) not found in bulk sulfate solutions is not surprising. The similar observations but different interpretations have been reported very recently[27,28] indicating that further studies of this system are necessary.

The accumulation of monovalent copper ions by the graphene electrode should lead to a concomitant decrease in water and sulfate ion coverage. This process can be probed by further looking at the oxygen K-edge PEEM data. Figure 3a-f presents a BLU treatment of a spectral intensity vs. time dataset for a fixed excitation energy of 541 eV (oxygen K-edge) for the same sample. As before, the background component (Fig. 3d, e, f) is limited to the aperture and empty cells, and is featureless. The electrochemically active component (Fig. 3b) is present in several electrolyte-filled channels, and its endmember (Fig. 3b and 3c) shows a strong ($\approx$ 8.8 %) signal increase at positive potentials. Oxidation of Cu^+ ions and product removal from the membrane's vicinity, as well as adsorption of HSO_4^- and SO_4^{2-} ions on graphene, must be responsible for the observed correlation. Spectroscopic data col-

3

lected from the same area were unmixed into two components, of which the active one is shown in Figures 3g (loading map highlighting electrolyte-filled channels) and 3h (corresponding endmember). The spectral endmember shows the main absorption peak at ≈541 eV, with a pre-edge shoulder by around 1 eV lower. Apart from this peak, all the other spectral features are also present in the reference spectrum measured on powdered hydrated and anhydrous $CuSO_4$ samples (Fig. 3i).
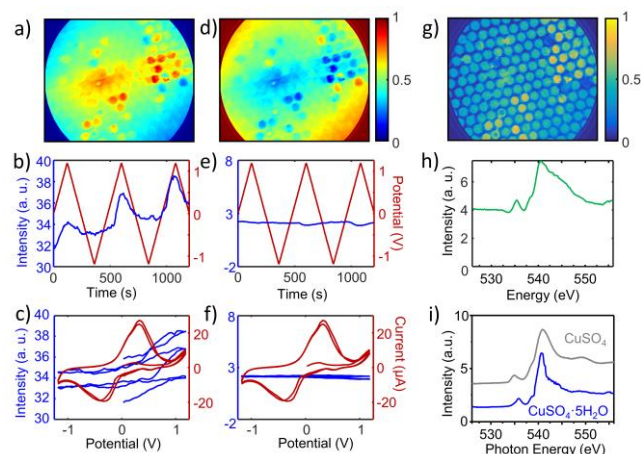

Figure 3. Oxygen K-edge data. Temporal dataset: (a) and (d) are the BLU abundance maps of the electrochemically active and inert background components, respectively; (b) and (e) are the corresponding BLU endmember components (PEEM intensity vs. time) plotted together with the WE potential variation; (c) and (f) are the same endmembers plotted vs. voltage and 2.5 cycles CV's recorded for the whole sample; the first cycle CV peaks are at 0.32 V and -0.41 V, for the second cycle peaks are at 0.33 V and -0.33 V; Spectral dataset: (g) is the BLU abundance map of a spectral dataset around oxygen K-edge (for complete BLU of this dataset, see SI, Fig. S2); (h) is the corresponding BLU endmember spectrum. (i) Reference oxygen K-edge spectra of anhydrous $CuSO_4$ and $CuSO_4 \cdot 5H_2O$ powdered samples.

Another interesting aspect arising from the voltammetry measurements is the correlation between the measured PEEM intensity at the O K-edge and the total amount of charge passed through the system. Apart from the pronounced oscillatory behavior present in Figure 3b, the cycle-to-cycle variations exhibit an independent rising trend (see Fig. S5). The explanation of these deviations from the perfect oscillatory behavior in both electrical and PEEM data can be caused by irreversible adsorption of HSO_4^-/SO_4^{2-} ions onto the graphene electrode or/and a slow evaporation of the solute causing an increase in the concentration of ions. The latter may lead to higher measured currents at the same applied potentials.

To conclude, we demonstrate probing of electrochemical reactions in an aqueous electrolyte using PEEM imaging and X-ray absorption spectroscopy. The observed spectroscopic signatures near the Cu L_3-edge are affected by the WE potential in a way consistent with copper (II) ion reduction on the graphene electrode. We show that although the Cu^+ ion is unstable in non-complexing media in the bulk of solution it can be present at the graphene surface, where the PEEM signal originates. The O K-edge response is likewise sensitive to graphene potential, which may reveal sorption of sulfate ions. We believe, that the use of graphene-capped multichannel array platform for PEEM imaging of in-liquid electrochemistry coupled with effective data mining algorithms such as BLU and combinatorial analysis is suitable for many applications dealing liquid-solid-gas interfacial analysis relevant to catalysis, energy, bio-medical research, ultrafast PEEM spectromicroscopy[29], plasmonics[30] and magnetizm[31].

ASSOCIATED CONTENT

Supporting Information

Further information on the MCA preparation, energy calibration, peaks assignment, copper electroplating, electrochemical characterization of MCA's, and complete BLU results of data of Figure 3g-h are available (PDF).

AUTHOR INFORMATION

Corresponding Authors

E-mail: s.nemsak@fz-juelich.de
E-mail: evgheni.strelcov@nist.gov
E-mail: andrei.kolmakov@nist.gov

Present Addresses

†If an author's address is different than the one given in the affiliation line, this information may be included here.

Notes

The authors declare no competing financial interest.

ACKNOWLEDGMENT

REFERENCES

(1)   Zaera, F. *Chemical Reviews* **2012**, *112*, 2920.

(2)   Salmeron, M.; Schlögl, R. *Surf Sci Rep* **2008**, *63*, 169.

(3)   Nemšák, S.; Shavorskiy, A.; Karslioglu, O.; Zegkinoglou, I.; Rattanachata, A.; Conlon, C. S.; Keqi, A.; Greene, P. K.; Burks, E. C.; Salmassi, F.; Gullikson, E. M.; Yang, S.-H.; Liu, K.; Bluhm, H.; Fadley, C. S. *Nature Communications* **2014**, 5, 5441.

(4)   Favaro, M.; Jeong, B.; Ross, P. N.; Yano, J.; Hussain, Z.; Liu, Z.; Crumlin, E. J. *Nature Communications* **2016**, 7, 12695.

(5)   Velasco-Velez, J. J.; Pfeifer, V.; Hävecker, M.; Weatherup, R. S.; Arrigo, R.; Chuang, C.-H.; Stotz, E.; Weinberg, G.; Salmeron, M.; Schlögl, R.; Knop-Gericke, A. *Angewandte Chemie International Edition* **2015**, *54*, 14554.

(6)   Locatelli, A.; Bauer, E. *Journal of Physics: Condensed Matter* **2008**, *20*, 093002.

(7)   Starr, D. E.; Liu, Z.; Havecker, M.; Knop-Gericke, A.; Bluhm, H. *Chemical Society Reviews* **2013**, *42*, 5833.

(8)   Rotermund, H. H.; Engel, W.; Jakubith, S.; Vonoertzen, A.; Ertl, G. *Ultramicroscopy* **1991**, *36*, 164.

(9)   Stasio, G. D.; Gilbert, B.; Nelson, T.; Hansen, R.; Wallace, J.; Mercanti, D.; Capozi, M.; Baudat, P. A.; Perfetti, P.; Margaritondo, G.; Tonner, B. P. *Review of Scientific Instruments* **2000**, *71*, 11.

(10)   Panzer, D.; Beck, C.; Maul, J.; Möller, M.; Decker, H.; Schönhense, G. *European Biophysics Journal* **2008**, *38*, 53.

(11)   Kolmakov, A.; Dikin, D. A.; Cote, L. J.; Huang, J.; Abyaneh, M. K.; Amati, M.; Gregoratti, L.; Gunther, S.; Kiskinova, M. *Nat Nano* **2011**, *6*, 651.

(12)   Guo, H.; Strelcov, E.; Yulaev, A.; Wang, J.; Appathurai, N.; Urquhart, S.; Vinson, J.; Sahu, S.; Zwolak, M.; Kolmakov, A. *Nano Letters* **2017**, *17*, 1034.

(13)   Yulaev, A.; Guo, H.; Strelcov, E.; Chen, L.; Vlassiouk, I.; Kolmakov, A. *ACS Applyed Materials and Interfaces* **2017**, *9*, 26492.

(14)   Greiner, M. T.; Jones, T. E.; Johnson, B. E.; Rocha, T. C. R.; Wang, Z. J.; Armbruster, M.; Willinger, M.; Knop-Gericke, A.; Schlogl, R. *Physical Chemistry Chemical Physics* **2015**, *17*, 25073.

(15)   Gurevich, A. B.; Bent, B. E.; Teplyakov, A. V.; Chen, J. G. *Surface Science* **1999**, *442*, L971.

(16)   Grioni, M.; Vanacker, J. F.; Czyzyk, M. T.; Fuggle, J. C. *Physical Review B* **1992**, *45*, 3309.

(17)   Szilagyi, R. K.; Frank, P.; DeBeer George, S.; Hedman, B.; Hodgson, K. O. *Inorganic Chemistry* **2004**, *43*, 8318.

(18)   Dobigeon, N.; Moussaoui, S.; Coulon, M.; Tourneret, J. Y.; Hero, A. O. *IEEE Transactions on Signal Processing* **2009**, *57*, 4355.

(19)   Strelcov, E.; Belianinov, A.; Hsieh, Y.-H.; Jesse, S.; Baddorf, A. P.; Chu, Y.-H.; Kalinin, S. V. *ACS Nano* **2014**, *8*, 6449.

(20)   Milchev, A.; Zapryanova, T. *Electrochimica Acta* **2006**, *51*, 2926.

(21)   Beverskog, B.; Puigdomenech, I. *Journal of The Electrochemical Society* **1997**, *144*, 3476.

(22)   Vereecken, P. M.; Binstead, R. A.; Deligianni, H.; Andricacos, P. C. *IBM Journal of Research and Development* **2005**, *49*, 3.

(23)   Chiu, Y.-D.; Dow, W.-P.; Huang, S.-M.; Yau, S.-L.; Lee, Y.-L. *Journal of The Electrochemical Society* **2011**, *158*, D290.

(24)   De la Pena, F.; Barrett, N.; Zagonel, L.; Walls, M.; Renault, O. *Surface Science* **2010**, *604*, 1628.

(25)   Brownson, D. A. C.; Kampouris, D. K.; Banks, C. E. *Chemical Society Reviews* **2012**, *41*, 6944.

(26)   Vazquez-Arenas, J.; Vázquez, G.; Meléndez, A. M.; González, I. *Journal of The Electrochemical Society* **2007**, *154*, D473.

(27)   Velasco Vélez, J. J.; Skorupska, K.; Frei, E.; Huang, Y.-C.; Dong, C. L.; Su, B.-J.; Hsu, C.-J.; Chou, H.-Y.; Chen, J.-M.; Strasser, P. *The Journal of Physical Chemistry B* **2017**.

(28)   Weatherup, R. S.; Wu, C. H.; Escudero, C.; Pérez-Dieste, V.; Salmeron, M. B. *The Journal of Physical Chemistry B* **2017**.

(29)   Man, M. K.; Margiolakis, A.; Deckoff-Jones, S.; Harada, T.; Wong, E. L.; Krishna, M. B. M.; Madéo, J.; Winchester, A.; Lei, S.; Vajtai, R.; Ajayan, P. M.; Dani, K. M. *Nature nanotechnology* **2017**, *12*, 36.

(30)   Dąbrowski, M.; Dai, Y.; Petek, H. *The Journal of Physical Chemistry Letters* **2017**, *8*, 4446.

(31)   Cinchetti, M.; Albaneda, M. S.; Hoffmann, D.; Roth, T.; Wüstenberg, J.-P.; Krauß, M.; Andreyev, O.; Schneider, H.; Bauer, M.; Aeschlimann, M. *Physical review letters* **2006**, *97*, 177201.

TOC figure